Molecular codes and in vitro generation of hypocretin and melanin concentrating hormone neurons

Ali Seifinejad[a,b,1], Sha Li[a], Cyril Mikhail[b], Anne Vassalli[a], Sylvain Pradervand[c], Yoan Arribat[a], Hassan Pezeshgi Modarres[d], Bridget Allen[e], Rosalind M. John[e], Francesca Amati[a], and Mehdi Tafti[a,1]

[a]Department of Physiology, Faculty of Biology and Medicine, University of Lausanne, 1005 Lausanne, Switzerland; [b]Center for Integrative Genomics, Faculty of Biology and Medicine, University of Lausanne, 1015 Lausanne, Switzerland; [c]Genomic Technologies Facility, Faculty of Biology and Medicine, University of Lausanne, 1015 Lausanne, Switzerland; [d]Institute of Bioengineering, School of Life Sciences, Ecole Polytechnique Fédérale de Lausanne, 1015 Lausanne, Switzerland; and [e]Biomedicine Division, Cardiff School of Biosciences, Cardiff University, CF10 3AX Cardiff, United Kingdom

Edited by Joseph S. Takahashi, University of Texas Southwestern Medical Center, Dallas, TX, and approved July 10, 2019 (received for review February 8, 2019)

Hypocretin/orexin (HCRT) and melanin concentrating hormone (MCH) neuropeptides are exclusively produced by the lateral hypothalamus and play important roles in sleep, metabolism, reward, and motivation. Loss of HCRT (ligands or receptors) causes the sleep disorder narcolepsy with cataplexy in humans and in animal models. How these neuropeptides are produced and involved in diverse functions remain unknown. Here, we developed methods to sort and purify HCRT and MCH neurons from the mouse late embryonic hypothalamus. RNA sequencing revealed key factors of fate determination for HCRT (*Peg3*, *Ahr1*, *Six6*, *Nr2f2*, and *Prrx1*) and MCH (*Lmx1*, *Gbx2*, and *Peg3*) neurons. Loss of *Peg3* in mice significantly reduces HCRT and MCH cell numbers, while knock-down of a *Peg3* ortholog in zebrafish completely abolishes their expression, resulting in a 2-fold increase in sleep amount. We also found that loss of HCRT neurons in *Hcrt-ataxin-3* mice results in a specific 50% decrease in another orexigenic neuropeptide, QRFP, that might explain the metabolic syndrome in narcolepsy. The transcriptome results were used to develop protocols for the production of HCRT and MCH neurons from induced pluripotent stem cells and ascorbic acid was found necessary for HCRT and BMP7 for MCH cell differentiation. Our results provide a platform to understand the development and expression of HCRT and MCH and their multiple functions in health and disease.

HCRT/OREXIN | MCH | transcription factor | iPSC | Peg3

The lateral and posterior hypothalamus play a central role in the regulation of food intake (1), vigilance states (2, 3), reward, and motivation (4). Among major cell types of this region are hypocretin/orexin- (HCRT) and melanin concentrating hormone- (MCH) producing cells. These neuropeptides are not colocalized but their cells are spatially intermingled (5).

HCRT and MCH neurons send projections throughout the central nervous system (CNS) (6, 7) and orchestrate their effects via their respective receptors; HCRT receptor 1 and 2 and MCH receptor 1 and 2 (8, 9). HCRT neurons project to all wake-promoting nuclei of the brain located in the brainstem, basal forebrain, hypothalamus, and thalamus (7). As physiological integrators they act as intermediates between different regulatory pathways, such as the autonomic, endocrine, feeding, reward, and stress systems (10, 11). MCH neurons are also involved in multiple functions including sleep, especially rapid-eye movement sleep (12), regulating energy balance (13), beat frequency of ependymal cilia, and ventricular volume (14), and are associated in controlling stress, and learning and memory (15, 16).

There is considerable evidence that sleep disorders are lined to alteration in HCRT signaling. Narcolepsy in dogs is linked to recessive loss-of-function mutations in HCRT receptor 2 (17). Patients with narcolepsy with cataplexy (also called narcolepsy type1 or NT1) have reduced or undetectable cerebrospinal fluid levels of HCRT-1 peptide and immunostaining of postmortem hypothalami shows no or dramatically reduced HCRT cells, while MCH cells are intact (18). Hypocretin deficiency is accompanied by sudden loss of muscle tone (cataplexy) and daytime sleepiness, the 2 main features of narcolepsy with cataplexy. In addition, *Hcrt* gene deletion in mice results in a phenotype similar to human narcolepsy (19). How narcolepsy patients lose the expression of the *Hcrt* gene or HCRT cells remains a mystery, but one hypothesis is an autoimmune-driven destruction of HCRT cells (20). The specific peptide expressed by HCRT cells and targeted by the immune attack is unknown, although autoreactive T cells to HCRT were recently reported (21) in narcolepsy with and without cataplexy. The important role of MCH in the pathophysiology of obesity, especially diet-induced obesity, is proven (9, 13, 22). How these multiple functions are accomplished by a small number of hypothalamic neuronal cell types needs careful investigation of their intrinsic properties.

Transcriptional maps for MCH cells were lacking until very recently (23) and attempts to obtain profiles for HCRT neurons relied on total RNA or mRNA of HCRT cells through transcript precipitation and comparing brains with and without HCRT (24–27), except in the recent single-cell transcriptome study (23). For the mRNAs obtained from HCRT neurons, some portion of transcripts is lost due to technical problems and because transcripts are not precipitated from purified cells. In the comparative study between HCRT-deficient and normal brain tissues, the differentially expressed genes (DEGs) can be masked by transcripts of other cell types. Finally, microarray technology was used to

Significance

Hypocretin (HCRT) and melanin concentrating hormone are brain neuropeptides involved in multiple functions, including sleep and metabolism. Loss of HCRT causes the sleep disorder narcolepsy. To understand how these neuropeptides are produced and contribute to diverse functions in health and disease, we purified their cells from mouse embryonic brains and established their molecular machinery. We discovered that partial removal of PEG3 (a transcription factor) in mice significantly reduces the number of HCRT and melanin concentrating hormone neurons, and its down-regulation in zebrafish completely abolishes their expression. We used our molecular data to produce these neurons in vitro from mouse fibroblasts, a technique that can be applied to cells from narcolepsy patients to generate an in vitro cell-based model.

Author contributions: A.S., R.M.J., F.A., and M.T. designed research; A.S., S.L., C.M., Y.A., and B.A. performed research; A.S., S.L., A.V., S.P., Y.A., H.P.M., and M.T. analyzed data; and A.S., A.V., R.M.J., and M.T. wrote the paper.

The authors declare no conflict of interest.

This article is a PNAS Direct Submission.

Data deposition: The data reported in this paper have been deposited in the Gene Expression Omnibus (GEO) database, https://www.ncbi.nlm.nih.gov/geo (accession nos. GSE126330 and GSE126345).

[1]To whom correspondence may be addressed. Email: Ali.Seifinejad@unil.ch or Mehdi.Tafti@unil.ch.

This article contains supporting information online at www.pnas.org/lookup/suppl/doi:10.1073/pnas.1902148116/-/DCSupplemental.

compare the samples, which is less sensitive than RNA sequencing (RNA-seq), a technique that allows the detection of differentially spliced transcripts and transcripts with low abundance. In zebrafish, RNA-seq was used on purified HCRT cells and led to the identification of the *Kcnh4a* gene, which has a sleep modulatory role (28). Complementary to these approaches, emerging technologies, like single-cell sequencing of specific (MCH and HCRT) (29) or whole LH cell types (23), have substantially improved our understanding of molecular properties of these cell types in the adult mouse brain.

We hypothesized that a specific transcriptional machinery is responsible for the unique features of HCRT and MCH cells. To identify molecules that orchestrate the early specification of these cell types and to characterize molecules unique to them, we purified these cells from the mouse brain. We identified a set of transcription factors (TF) with important roles in the fate determination of both HCRT and MCH cells. One of these, PEG3, was identified with a substantial role in regulating vigilance states. The result of this high-throughput study and the discovery of these specific TFs led us to develop a protocol to derive these neuronal populations from mouse fibroblasts, that could potentially be applied to human cells to establish an in vitro model or for cell-replacement therapy in narcolepsy with cataplexy. Through this process, we have also identified molecules with potential importance in understanding the pathophysiology of narcolepsy.

Result

Transcriptome Analysis of Different Brain Areas in *Hcrt* Gene-, or Hcrt Cell-, Ablated Mice Reveals *Qrfp* as a Putative Marker of Narcolepsy with Cataplexy. To identify cell type-specific regulators of HCRT cells, we used 2 mouse models of narcolepsy with cataplexy: *Hcrt* gene knockout ($Hcrt^{ko/ko}$) mice (19) and *Hcrt-ataxin-3* mice in which HCRT cells are ablated by the expression of the *ataxin-3* gene (30). We hypothesized that comparing the brain transcriptome of these mice and their controls might identify transcriptional changes due both to a lack of the *Hcrt* gene and HCRT neurons altogether (as in narcolepsy). We dissected the hypothalamus, brainstem, and neocortex of adult mice belonging to 4 genotype groups: $Hcrt^{ko/ko}$ and $Hcrt^{+/+}$ littermates, and *Hcrt-Ataxin-3* hemizygous transgenic (Tg^{+}) and WT littermates. RNA was purified and submitted to high-throughput RNA-seq.

As expected, the *Hcrt* transcript was found to be severely depleted in the hypothalamus of $Hcrt^{ko/ko}$ and *Hcrt-ataxin-3* transgenic mice (Fig. 1*A*). Nevertheless, very few DEGs except *Hcrt* were identified (adjusted $P < 0.05$) (*SI Appendix*, Table S1). Analysis showed that in the cortex of $Hcrt^{ko/ko}$ mice *Kcnh4* and *Krt12* gene transcripts were down-regulated by more than 2-fold. *Kcnh4* encodes a voltage-gated potassium channel proposed to play a role in sleep regulation in zebrafish (28). In *Hcrt-Ataxin-3* mice, comparing all 3 brain areas with respective controls identified the *Cenpc1* gene with significant up-regulation in transgenic animals (Fig. 1*B*). *Cenpc1* encodes a protein that modulates DNA methylation and the histone code at centromeric regions (31).

One of the very few genes that were affected by HCRT cell loss in *Hcrt-Ataxin-3* but not *Hcrt* gene deletion was *Qrfp*, which attracted our attention due to its neuropeptidergic identity and anorexigenic function. *Hcrt-Ataxin-3* Tg^{+} mice exhibited a 50% decrease in *Qrfp* transcript levels in their hypothalamus relative to controls, while levels in $Hcrt^{ko/ko}$ mice did not differ from WT littermates (Fig. 1*C*). To confirm *Hcrt-ataxin-3* Tg^{+} mice hypothalamic *Qrfp* reduction, the hypothalamus was dissected at the age of 1, 3, 6, and 9 wk, and analyzed by qRT-PCR. A massive reduction of *Hcrt* gene expression during all ages was observed, while there were no changes in *Pmch* gene expression (Fig. 1 *D* and *E*). More than 50% reduction was observed in *Qrfp* gene expression at all ages (1 wk: WT = 0.9 ± 0.07 vs. tg = 0.31 ± 0.05, $P < 0.01$; 3 wk: WT = 2.9 ± 0.2 vs. tg = 0.9 ± 0.06, $P < 0.01$; 6 wk: WT = 1.8 ± 0.1 vs. tg = 0.6 ± 0.04, $P < 0.01$; 9 wk: WT = 1.8 ± 0.1 vs. tg = 0.7 ± 0.06, $P < 0.05$; *t* test) (Fig. 1*F*). It was shown in zebrafish and mouse that QRFP and HCRT most probably comprise different subgroups of hypothalamic cells with no colocalization (25, 32). Nevertheless, single-cell RNA-seq analysis of the hypothalamus indicated colocalization of *Qrfp* and *Hcrt* and hierarchical clustering of hypothalamic neuronal subtypes defined by unique molecular fingerprints showed *Hcrt* and *Qrfp* among the closest neuronal subtypes, with the difference that QRFP neurons also highly express brain-derived neurotrophic factor (33). Our finding that *Qrfp* is lost together with HCRT neurons in *Hcrt*-ablated mice suggests that *Qrfp* might play a role not only in the control of sleep and metabolism but potentially in narcolepsy.

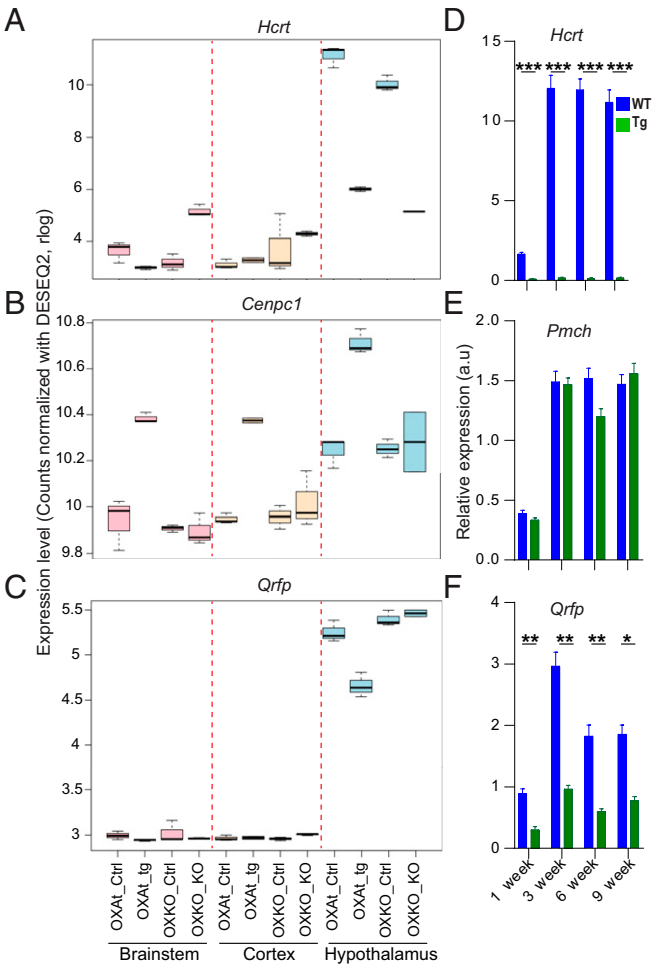

Fig. 1. Identification of *Cenpc1* and *Qrfp* as putative narcolepsy gene markers. (*A–C*) Differential RNA sequencing analysis between $Hcrt^{ko/ko}$ (OXKO), or *Hcrt-Ataxin-3 Tg* (OXAt) mice, and their respective control littermates (Ctrl), was performed in 3 brain regions (brainstem, cortex, and hypothalamus). Depicted are the differential expressions of *Hcrt*, *Cenpc1*, and *Qrfp* in each region. Note that *Qrfp* mRNA levels are about 50% reduced in the hypothalamus of *Hcrt-ataxin-3* transgenic mice relative to WT littermates. Read counts has been normalized with DESeq2 package. (*D–F*) Expression of *Hcrt*, *Pmch*, and *Qrfp* in the hypothalamus of *Hcrt-Ataxin-3* transgenic and WT littermates at 4 developmental time points (1, 3, 6, and 9 wk after birth). Shown are values (mean ± SEM, arbitrary units) derived from qRT-PCR analysis (*t* test, $n = 3$ mice; $^{*}P = 0.023$; $^{**}P < 0.01$; $^{***}P < 0.001$).

Sorting of Intact Lateral Hypothalamic Cells. Despite the discovery of *Qrfp*, the above experiment suffers several shortcomings as described in our introduction. To define the specific transcriptional repertoires of HCRT and MCH neurons, we set out to purify each cell type, and compare their transcriptomes to the rest of hypothalamus and to each other. Cell survival rate was too low during and after sorting of adult brains, while it was feasible for late embryonic stages (embryonic day [E] 18 to E19).

We established a protocol in which the hypothalamus of E18 to E19 *Hcrt-Cre* transgenic (34) or C57BL/6J mice embryos were dissected and dissociated single hypothalamic cells were prepared and transduced with viral vectors with reporter proteins (Fig. 2*A* and *SI Appendix*, *Supplementary Information Text*). The challenging issue was the purification of HCRT cells due to the low number of cells and the low expression level of the *Hcrt* gene at this developmental stage. Therefore, regular reporter markers, like eGFP in *Orexin-eGFP* mice (35), are not suitable. To improve the sorting, we set up a system enabling the amplification of the reporter gene. We took advantage of an adeno-associated virus (AAV) vector where an *mCherry* gene is inserted downstream of *Eef1a1* promoter in the opposite orientation between 2 loxP sites (Fig. 2*B*). The neurobasal medium containing cells and viral vector were dispensed in low adherent 96-well plates. This method forces cells to quickly aggregate, which improves tremendously the survival rate (Fig. 2*A*). Aggregates were kept in neurosphere medium for 7 d to allow mCherry accumulation and cell sorting (Fig. 2*C*). We were able to sort 234.87 ± 126.29 $mCherry^+$ cells from each E18 to E19 brain and collected about more than 5,000 cells for each biological replicate (3 replicates of $mCherry^+$ and 3 $mCherry^-$) (*SI Appendix*, Fig. S1*A*). A total amount of high-quality RNA, ranging from 1 to 2.5 ng, was extracted from samples (*SI Appendix*, Fig. S1*C*) and RNA-seq was performed to identify DEGs.

To purify the MCH cells, which show enough E18 to E19 expression level, we isolated them based on the level of EGFP expression. To this end, we inserted the *eGFP* sequence between 2 long-terminal repeats of the pRRLSIN lentiviral backbone under the mouse *Pmch* gene promoter and the *mCherry* sequence under the human *PGK* promoter (Fig. 2*D*). To verify if the lentivector acts specifically, we transduced the hypothalamus, cortex, and cortex+hippocampus cell cultures. One week later the cultures were stained for the expression of EGFP and MCH. Only in hypothalamic cultures was the expression and colocalization of both peptides detected, indicating that our construct is specific (Fig. 2*E*). MCH cells were sorted based on this lentiviral system and approximately the same number of cells was sorted and high-quality RNA was extracted for RNA-seq.

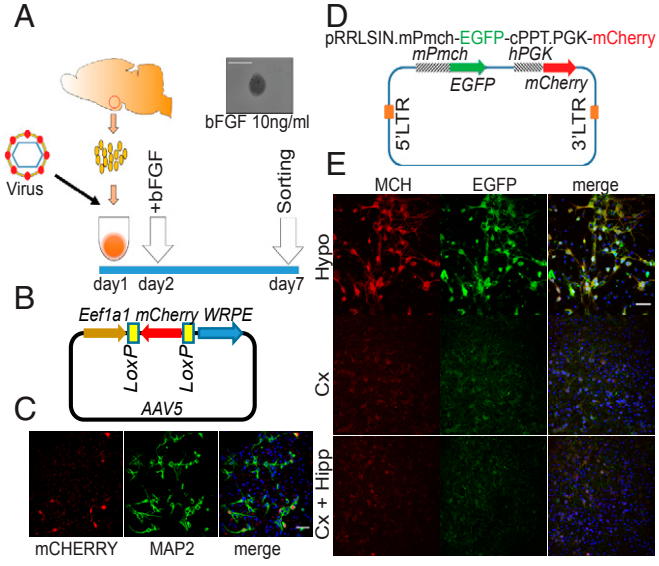

Fig. 2. Methods for isolation of HCRT and MCH neurons. (*A*) Schematic of the method used for the isolation of hypothalamic cells. *Hcrt-Cre* transgenic mice and *C57BL/6J* mice were used to purify HCRT and MCH cells, respectively. In this method, dissociated hypothalamic cells are dispensed in low adherent 96-well plates inside neurosphere medium containing viral vectors. Addition of bFGF from day 2 is helpful for survival rate. (*B*) AAV construct used for purification of HCRT cells from *Hcrt-Cre* embryonic mice brain. In this viral vector the expression of *mCherry* requires Cre recombinase. (*C*) Cultured E18 hypothalamic cells isolated from *Hcrt-Cre* transgenic mice, after transduction with AAV carrying the *mCherry* gene, accumulate enough expression of mCherry within 7 d. (*D*) Dual reporter lentiviral construct for the purification of MCH cells. (*E*) Embryonic cultures of hypothalamus (Hypo), cortex (Cx) and cortex and hippocampus (Cx+Hipp) were transduced with dual reporter lentiviral vector. After 7 d, MCH and EGFP are only detected in the hypothalamus where MCH cells belong. (Scale bars: 50 μm.)

Identification of Enriched Genes by FACS Sorting of HCRT and MCH Cells. As expected, RNA-seq results showed a large enrichment of read counts for *mCherry* RNA in HCRT cells ($mCherry^+$ = 67.1 ± 21.9 vs. $mCherry^-$ = 11.2 ± 1.9, counts per million reads [cpm], mean ± SEM) and for EGFP in MCH cells ($EGFP^+$ = 82.5 ± 2.4 vs. $EGFP^-$ = 15.6 ± 0.25, cpm, mean ± SEM) (Fig. 3 *A* and *B*). This analysis revealed 652 DEGs, among them 350 genes up-regulated in HCRT cells by more than 2-fold. In addition to *Hcrt*, *Pdyn* (3-fold increase), *Dlk1* (4.5-fold increase), and *Adra2a* (3-fold increase) are known markers of HCRT cells (24). We also identified 2,665 DEGs in MCH cells compared with other hypothalamic cell types; 468 of them were up-regulated more than 2-fold (Fig. 3 *C* and *D* and *SI Appendix*, Table S2). A higher number of DEGs for MCH neurons might be due to the fact that these neurons appear to be more mature at E18 to E19 than HCRT neurons. In silico verification (Allen atlas) of the expression of some of these DEGs confirmed hypothalamic and lateral hypothalamic expression patterns in the adult mouse brain (*SI Appendix*, Fig. S2). We also confirmed the colocalization of some of these genes with HCRT and MCH by immunohistochemistry (Fig. 3*E*).

Unique Gene Sets Distinguish HCRT and MCH Cell Types. We identified 2 gene sets which might underlie the unique characteristics of these 2 cell types: (*i*) a set of genes with TF and DNA binding activity, and (*ii*) specific genes that are part of some important pathways and are differentially regulated between the 2 cell types.

Eighteen genes with DNA binding and TF activity were up-regulated more than 2-fold in HCRT cells and 18 in MCH cells. Only *Ldb2* and *Ahr* were shared between the 2 cell types, with the remaining TFs being cell-type specific (Fig. 4*A* and *SI Appendix*, Table S3). *Lhx9*, proposed as a regulator of HCRT cell development (24, 25, 36), was not significantly changed between cell types. Of the other *Lhx* gene family members, only *Lhx3* and *Lhx6* were less expressed in MCH cells (*SI Appendix*, Table S2).

Pathway analysis for differentially regulated genes highlighted signaling, disease, and metabolic pathways. In this analysis, we included all significantly differentially regulated genes and identified shared but differential pathways between the 2 cell types. The gene list with opposite direction of expression is shown in Fig. 4*B*. These genes have exosomal, hormonal, and signaling but mainly unknown functions and have lateral hypothalamic expression. Pathway analysis indicated that some of these genes are involved in infectious diseases, autoimmune thyroid disease, mRNA surveillance, amyotrophic lateral sclerosis, and the PI3K-Akt signaling pathway (*SI Appendix*, Table S4). Opposite direction of expression of these genes in the 2 cell types might also explain their opposite contribution to behaviors, such as sleep (HCRT promoting wakefulness and MCH sleep).

By analyzing the expression pattern of HCRT and MCH neurons with immunohistochemistry and with the mature neuronal marker NeuN (anti-NeuN antibody against purified nuclear proteins from mouse brain), we made a serendipitous discovery. HCRT neurons do not express the NeuN marker, while MCH neurons and other hypothalamic neurons do (Fig. 4*C*). To test the specificity of this finding we also tested another NeuN antibody (against the first 100 amino acids of the human NeuN) and found exactly the same lack of staining of HCRT neurons. This is surprising since NeuN is expressed by all CNS mature neurons except by Purkinje and Golgi cells of the cerebellum (37). NeuN is encoded

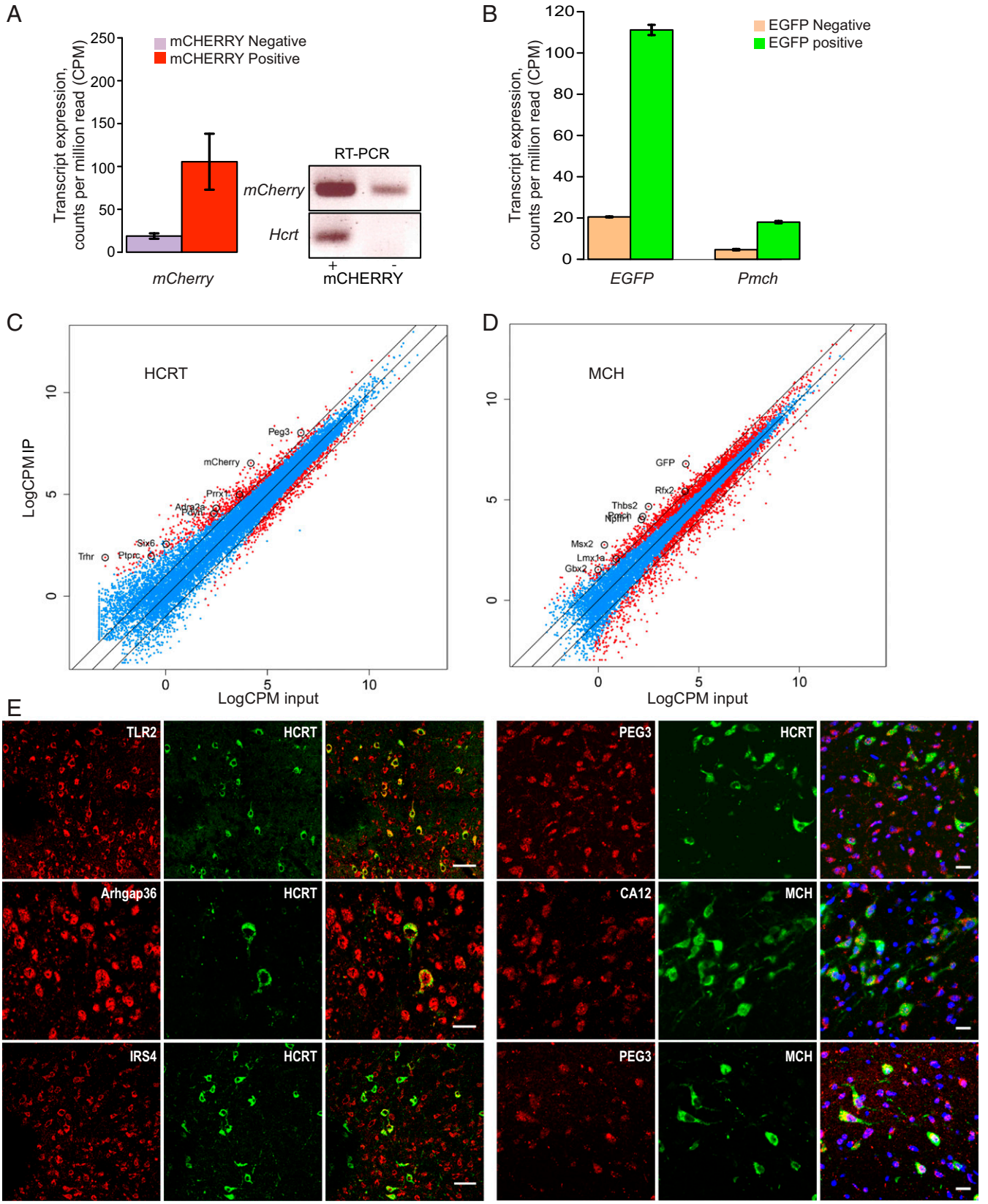

Fig. 3. Verification of the methods and enrichment for the genes expressed in HCRT and MCH cells. (*A*) HCRT cell sorting: cells sorted for mCherry fluorescence displayed enrichment for *Hcrt* transcript (*Left*). Due to very low expression of the *Hcrt* gene, we performed PCR to confirm the enrichment of HCRT cells and mCherry^{+} cells were also positive for *Hcrt* expression (*Right*). The results are RNA-seq results and the transcript expression level is displayed as cpm reads. (*B*) MCH cell sorting: EGFP enriched cells showed enrichment for *EGFP* and *Pmch* transcripts. (*C* and *D*) Plotting of log counts per million reads (LogCPM) of immunoprecipitation against LogCPM input. Significant DEG genes are highlighted in red and nonsignificant ones in blue ($P > 0.05$). Outer lines are 2-fold increase/decrease in expression. Some representative genes are marked. (*E*) Colocalization of candidate genes (red) with HCRT and MCH neuropeptides (green). (Scale bars: *Left*, 50 μm; *Right*, 20 μm.)

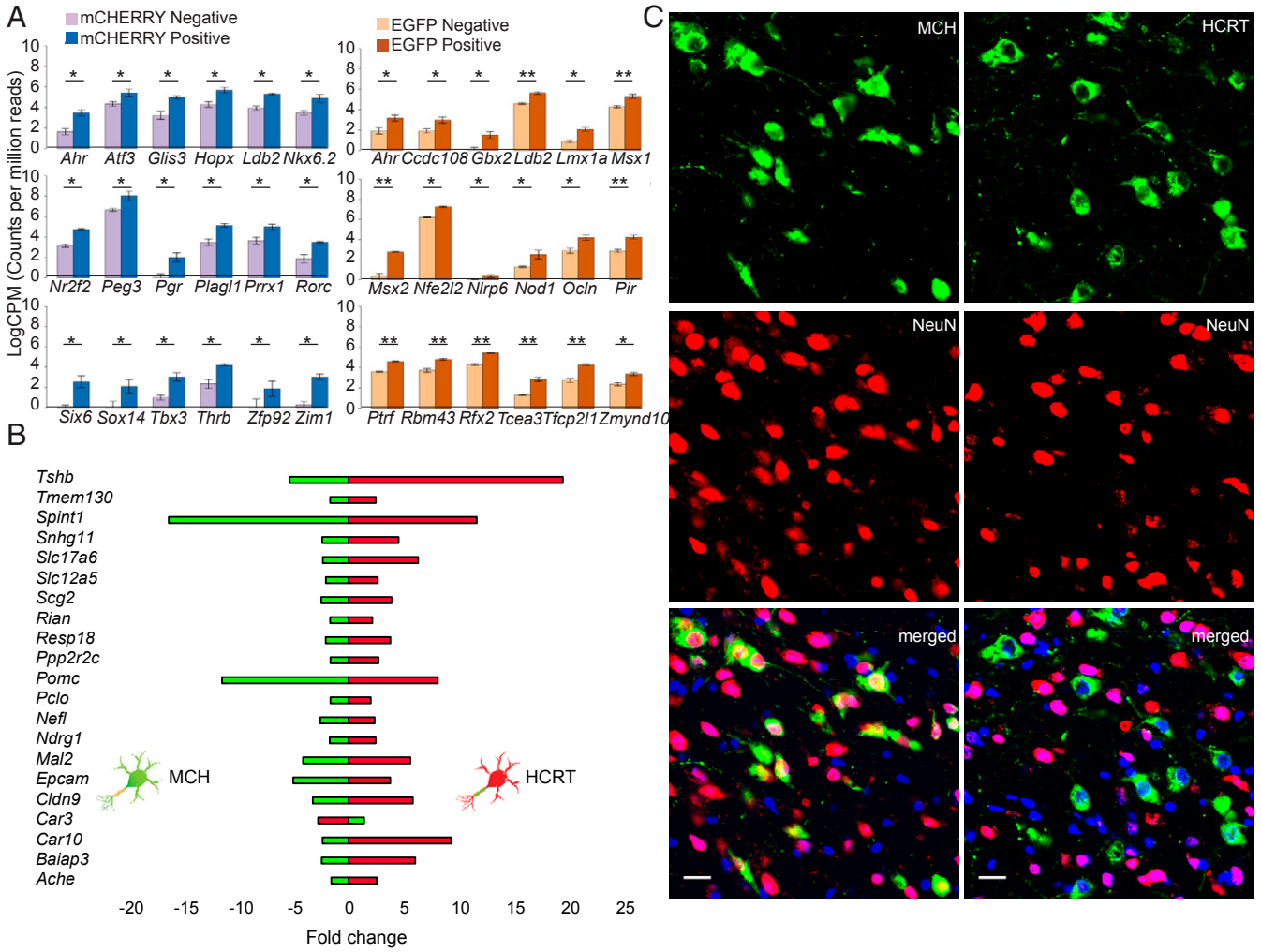

Fig. 4. Gene sets differentially expressed in HCRT versus MCH cells. (*A*) TFs enriched in HCRT (*Left*) and in MCH cells (*Right*). Positives are pure HCRT and MCH cells and negatives are other hypothalamic cells. Transcript expression is displayed as LogCPM. $*P < 0.05$; $**P < 0.01$; $n = 3$, mean ± SEM. (*B*) Gene set with opposite direction of expression between HCRT (green) and MCH (red) cell types. The graph shows fold-change in gene expression when HCRT and MCH cells' transcriptome are compared with the rest of the hypothalamus. (*C*) Immunostaining for colocalization of hypothalamic HCRT and MCH cells with NeuN neuronal marker. As shown MCH as many other surrounding cells express NeuN while HCRT cells do not. (Scale bars: 20 μm.)

by *Rbfox3* (38), a splicing regulator, suggesting that adult HCRT neurons might have a set of differentially spliced mRNAs.

Several ion channels and receptors were also identified for each cell type (*SI Appendix*, Fig. S3). Finally, we detected a strong up-regulation of the *Trhr* gene in HCRT cells and it is known that thyrotropin-releasing hormone (TRH) stimulates these neurons (39) (*SI Appendix*, Table S2).

Morpholino Knockdown of Candidate TFs. To identify a possible role of the candidate TFs to modulate *Hcrt* and *Pmch* gene expression, we knocked down their expression by morpholino oligonucleotides (Mo) (*SI Appendix*, *Supplementary Information Text* and Table S7) in zebrafish embryos at the 1-cell stage. Among candidate TFs, PEG3 is not found in the zebrafish genome. We therefore used its ortholog in *Danio rerio* (si:ch211-266d19.4; XM_009297216.2; zinc finger protein 271, *Zfp271*). Among 10 top TFs enriched in HCRT cells, Mo-*Zfp271* at 2.5 ng strikingly abolished *Hcrt* gene expression (Fig. 5 *A* and *B*) but did not result in an any developmental defect (Fig. 5A and *SI Appendix*, Fig. S4*A*). Mo-*Six6* (33%) and Mo-*Prrx1* (10%) at 1.25 ng also reduced *Hcrt* expression. At 2.5 ng, Mo-*Six6* (45%) and Mo-*Prrx1*(38%) had the most pronounced effect after Mo-*Zfp271*(100%), Mo-*Ahr* (57%), and Mo-*Nr2f2* (40%), indicating that HCRT cells might arise from the Six family-expressing domain of the embryonic hypothalamus (40). The phenotype obtained from knockdown of several TFs enriched in MCH cells was partial loss of MCH signal for Mo-*Gbx2*, Mo-*Lmx1a*, and Mo-*Msx2a* (50%, 60%, and 22% respectively) (*SI Appendix*, Fig. S4*B*). *Peg3* was not enriched in MCH neurons but to test if it has any effect on *Pmch* expression, we also injected Mo-*Zfp271* and surprisingly observed that it also totally abolished MCH expression (*SI Appendix*, Fig. S4*B*).

Altered Locomotor Activity and Sleep Architecture in *Zfp271* (*Peg3* Ortholog) Knocked-Down Zebrafish. Enrichment of *Peg3* in HCRT cells and its effect on the expression of HCRT and MCH neuropeptides suggested a potential involvement in sleep regulation. The effect of *Zfp271* knockdown on zebrafish behavior was assessed using a locomotor activity assay, as previously described (41, 42). Mo-*Zfp271* larvae exhibited significantly less locomotor activity mainly during daytime (day 1: WT = 42.6 ± 5.8 vs. Mo-*Zfp271* = 21.1 ± 2.7; $P < 0.01$, *t* test) (Fig. 5*C*). This reduction in activity is accompanied with 2-fold increase in sleep time during the day (day 1: WT = 24.2 ± 2.6 vs. Mo-*Zfp271* = 45.2 ± 1.5; day 2: WT = 28 ± 2.2 vs. Mo-*Zfp271* = 41.6 ± 1.4; $P < 0.0001$, *t* test) (Fig. 5*D*). Analysis of sleep bout number and duration showed that the increase in sleep amount is mainly due to increased bout

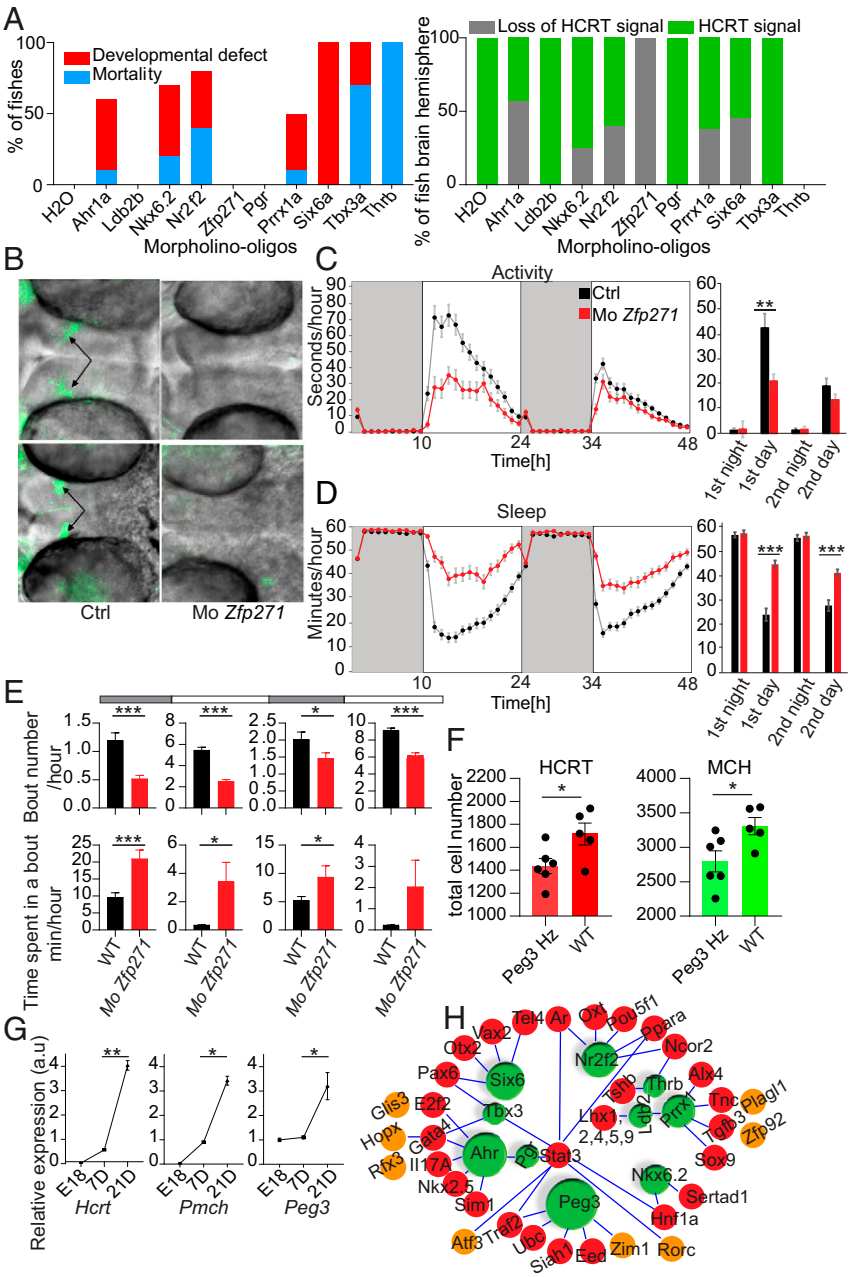

Fig. 5. Knockdown of critical TFs identified for *Hcrt* and *Pmch* gene expression and sleep behavior in fish. (*A*, *Left*) Mortality and developmental defect rate of 48-h postfertiliation zebrafish larvae injected with 2.5 ng of candidate Mo (*SI Appendix*, Table S7). Data are presented as percentage of fish that exhibit the phenotype ($10 < n < 20$). (*Right*) Visualization of HCRT signal in brain hemispheres of zebrafish embryos by immunostaining and confocal microscopy. The percentage of brain hemispheres positive or negative for HCRT signal for each candidate Mo is presented. (*B*) Representative image of loss of HCRT signal in Mo-*Zfp271*-injected zebrafish brains compared with controls. (10× confocal magnification.) (*C*) Hourly distribution of locomotor activity of *Zfp271* morphants and their respective controls during 48 h (night [10 h] and day [14 h]). Dark periods are indicated in gray and light periods in white. As shown in the bar graph (*Right*) Mo-*Zfp271*-injected zebrafish exhibit about 50% reduced locomotor activity during the light period. $^{**}P < 0.01$; $^{***}P < 0.001$. (*D*) Hourly distribution of sleep during 48 h. Mo-*Zfp271*-injected zebrafish exhibit profound increase in sleep time compared with controls. (*E*) Sleep bout numbers and bout durations in Mo-*Zfp271*-injected fish compared with controls. During both light and dark periods, *Zfp271* morphants exhibit reduced bout number. $^{*}P < 0.05$; $^{***}P < 0.001$; $n = 48$, mean ± SEM, *t* test. (*F*) HCRT and MCH neuron counts in *Peg3* hemizygous KO mice (Hz; *Peg3*$^{+/-}$) and their WT littermates. The entire hypothalamus was covered from anterior to posterior regions and all sections were counted. $^{*}P = 0.04$ for HCRT and $^{*}P = 0.02$ for MCH; total cell number ± SEM, Mann–Whitney *U* test; $n = 5$ to 6. (*G*) Quantitative PCR of brain *Hcrt*, *Pmch*, and *Peg3* expression during different time points. There is a parallel increase in the expression of *Hcrt* and *Pmch* along with *Peg3* up to 3 wk after birth. $^{*}P = 0.019$ for *Peg3* and $P = 0.03$ for *Pmch*; $^{**}P < 0.01$; $n = 3$, mean ± SEM; *t* test. (*H*) Potential gene network for identified TFs within HCRT cells. Their interactions are extracted from databases. The more effective TFs in zebrafish study (green) have bigger sizes. Identified TFs but not tested are in brown and potential targets in red.

duration both during the light (day 1: WT = 0.3 ± 0.02 vs. Mo-*Zfp271* = 3.4 ± 1.3; $P = 0.025$, *t* test) and the dark period (night 1: WT = 9.5 ± 1.3 vs. Mo-*Zfp271* = 20.9 ± 2.5, $P < 0.0001$; night 2: WT = 5.2 ± 0.6 vs. Mo-*Zfp271* = 9.3 ± 2, $P = 0.05$, *t* test) (Fig. 5*E*).

***Peg3* Loss-of-Function in Mice Reduces the Number of HCRT and MCH Cells.** *Peg3* is expressed from the paternal allele and female mice inheriting a targeted deletion of this allele display striking impairment of maternal behavior and decreased number of oxytocin neurons (43). In the same model system, we found a 16.31% decrease in the number of HCRT cells (WT [n = 5]:1716.4 ± 95.7 vs. KO [n = 6]: 1436.5 ± 66.39, mean ± SEM, $P = 0.04$, Mann–Whitney *U* test) and a 15.44% reduction in MCH cell number (WT [n = 5]: 3307.4 ± 123.6 vs. KO [n = 6]: 2796.5 ± 154.2, mean ± SEM, $P = 0.02$, Mann–Whitney *U* test) (Fig. 5*F*). These significant reductions confirmed a role for *Peg3* in regulating these critically important cell types.

We also investigated *Peg3* gene-expression levels in mice at different postnatal time points. The results showed that at postnatal day 21, when *Hcrt* and *Pmch* reach the peak of expression, *Peg3* also reaches its maximum level, indicating a strong temporal expression relationship between the 3 genes (Fig. 5*G*).

Transcriptome Data as a Roadmap to Generate MCH and HCRT Cells from Mouse Induced Pluripotent Stem Cells. To further understand the development of HCRT and MCH neurons, we aimed at establishing these neuronal cell types from pluripotent stem cells. We first focused on the generation of HCRT cells to monitor them easily in culture; we established induced pluripotent stem cells (iPSCs) from skin fibroblast of *Hcrt-eGFP* mice. This was performed by introducing 4 TFs (OCT3/4, SOX2, c-MYC, and KLF4) in fibroblasts and after 2 wk embryonic stem cell-like colonies were picked up and expanded. The colonies expressed known pluripotency markers (*SI Appendix*, Fig. S5 *A* and *C*) and silenced their transgenes, which normally should

occur after activation of internal stemness genes (*SI Appendix*, Fig. S5*B*). The established iPSCs also had strong potential to differentiate toward neural lineage (*SI Appendix*, Fig. S5*D*).

To differentiate our iPSCs toward hypothalamic neuronal progenitors, we took advantage of a protocol established by Wataya et al. (44). This method applies a strictly chemically defined medium with minimum level of inductive signals called "growth factor-free chemically defined medium" together with quick aggregation where the seeded cells are quickly precipitated in wells of low-adherent 96-well plates. Preliminary screening using this protocol with different conditions (more than 100 conditions) failed to induce *Hcrt* and *Pmch* gene expression (*SI Appendix*, Fig. S5*E*). Next, we tested if any specific signaling molecule can induce the expression of some TFs enriched in HCRT (*Peg3*, *Prrx1*, and *Six6*) and MCH (*Msx2*, *Lmx1a*, and *Rfx2*) cells from our RNA-seq experiment. To this end and based on the days that hypothalamic (*Rax* gene) and neuroepitelial (*Sox1* gene) markers start to be up-regulated during neuronal differentiation (Fig. 6*A*), we changed the protocol and from day 4 applied different signaling molecules and growth factors individually (*SI Appendix*, Fig. S5*F*). Screening of several molecules identified BMP7 as a highly potent molecule to induce the expression of TFs of interest (Fig. 6*B*). Almost all 6 TFs that were tested were strongly expressed in BMP7-treated cells (Fig. 6*B*). Intriguingly, BMP7 induced the expression of *Pmch* but not *Hcrt* gene (Fig. 6 *B–D*).

We next performed a detailed analysis of the effect of BMP7 on *Pmch* expression. Exposure of the neurospheres from day 4 showed that BMP7 exerts its effect 2 d after addition and *Pmch* expression is increased during several days (Fig. 6*C*). The effect of BMP7 was more pronounced only from day 4 (*SI Appendix*, Fig. S6*A*) and was dose-dependent (Fig. 6*E* and *SI Appendix*, Fig. S6*D*). Sonic hedgehog, which is one of the major regulators of hypothalamic patterning (45), was not able to induce *Pmch* expression, either in different media or at different concentrations (*SI Appendix*, Fig. S6*D*). The effect of the other members of BMP family, BMP4, was not as strong as BMP7 (*SI Appendix*, Fig. S6*B*). Addition of the retinoic acid, which is the important player for caudal CNS patterning (46), suppressed *Pmch* expression (*SI Appendix*, Fig. S6*C*). After 2 wk, the neurospheres were dissociated and cultured on coated dishes for 2 extra weeks to allow mature neuronal growth. Staining for MCH and MAP2 showed that MCH-expressing cells also express MAP2, indicating that these cells are mature neurons (Fig. 6*F*). We tested if any specific combination of TFs other than MCH cell-specific TFs, are affected by BMP7, which results in the induction of *Pmch* gene expression. qPCR analysis of about 30 candidate genes showed that, while genes from the *Pax* family are strongly down-regulated under BMP7 condition, *Rax*, an important hypothalamic marker, is highly expressed. *Six1* also showed increased expression. *Foxg1*, a major marker of telencephalon development, was strongly suppressed as expected (Fig. 6*G*). Based on our data and the literature, we propose a model to explain how different combinations of TFs might interact with each other and how their up- or down-regulation induces *Pmch* expression (Fig. 6*H*).

All above-mentioned approaches failed to induce any expression of HCRT, even though the treatment with BMP7 induced HCRT-enriched TFs (SIX6, PEG3, and PRRX1). We performed another large screen of molecules (*SI Appendix*, Fig. S6*E* and Table S5) and included vitamin C as one of the treatments. The reason for the inclusion of vitamin C was the enrichment of the *Gulo* (L-gulonolactone oxidase) gene in our HCRT cell RNA-seq experiment as well as our RNA-seq of *Hcrt-ataxin-3* mice (*SI Appendix*, Fig. S6*F*). L-Gulonolactone oxidase is the enzyme producing the precursor to ascorbic acid (47). Although a few of the screened molecules induced HCRT expression, only vitamin C treatment could be reproduced (*SI Appendix*, Fig. S6*G*). Inclusion of vitamin C in combination with different molecules showed its potential to induce the expression of the *Hcrt* gene (Fig. 6*I*). Vitamin C displays almost the same effect as ManNac, which has previously been shown to also induce the expression of *Hcrt* gene (48).

After plating the cells in poly-D-lysine (PDL)–coated dishes, EGFP-expressing neurons derived from *Hcrt-EGFP* iPSCs were detected in our cultures (Fig. 6*J*). To test if our in vitro MCH and HCRT cells are functional, we measured the secretion of their respective neuropeptide in the cell culture medium. MCH and HCRT cells plated on PDL dishes for 2 wk secreted about 96.61 ± 9.87 and 6.14 ± 1 pg/mL of their neuropeptides, respectively (Fig. 6*K*). After stimulation with an inducer molecule (TRH [125 nM] for HCRT cells and HCRT-1 [1 μM] for MCH cells), the levels increased to 115.35 ± 8.84 and 8.63 ± 0.38 pg/mL. Maturation stage also affects their functionality and more mature neurons showed more secretion of MCH (3-wk culture: 174.03 ± 31.67 vs. 2-wk culture: 96.61 ± 9.87 pg/mL) and HCRT (3-wk culture: 8.68 ± 2.3 vs. 2-wk culture: 6.14 ± 1 pg/mL, mean ± SEM, $n = 3$) neuropeptides (Fig. 6*K*).

Network of TFs in HCRT and MCH Cells. Partial or complete effect of the removal of a TF depends on the gene network. Based on the literature and different databases (BioGRID, TRRUST, and STRING), we predicted a potential network for the 18 identified TFs and their targets (physical and genetic interaction) in HCRT cells, which might explain the results of our knockdown experiment in zebrafish. PEG3 has the largest weight on the network since its removal totally abolishes HCRT expression (Fig. 5*H*). *Ldb2*, which showed no effect on the expression of the *Hcrt* gene when knocked down, has a direct interaction with the LHX protein family, which was shown to be necessary for a subset of HCRT neurons (24) (Fig. 5*H*). To have a broader view and to gain insight into how these cell types exert their multiple functions, we created a map of TFs to understand how different TFs assigned to different functions, like sleep or feeding, interact with each other. To this end, we used only experimentally available data in which these TFs were shown to display either physical or genetic interaction. The pool of TFs was chosen based on the following 3 criteria: (*i*) TFs up-regulated in our RNA-seq data, (*ii*) TFs regulating genes up-regulated more than 2-fold, and (*iii*) TFs with known functions in a specific behavior, such as FOXA2 (49) in feeding and LHX9 (24) and EBF2 (50) in sleep. For all TFs we also extracted if they have a salient role in a specific phenotype and if they are part of a specific pathway. Some TFs participated in known functions, such as development, sleep, and feeding behavior and obesity in both HCRT and MCH cells (*SI Appendix*, Fig. S7). Not only are there shared TFs between different functional groups, but they also interact with each other. Normally the output of this gene network is the expression or inhibition of *Hcrt*, *Pdyn* (Dynorphin), and glutamate for HCRT cells and the expression or inhibition of *Pmch* and *Gaba* for MCH cells, and proper functioning of these cell types (*SI Appendix*, Fig. S7). If these outputs are altered under different physiological and pathological conditions, it requires alteration in the gene network, as well. No TF can be excluded from any function but the figure presented here (*SI Appendix*, Fig. S7), which is based on available data, depicts some specifications. For example, the involvement of FOXA2 in feeding behavior might require different connections within the 2 cell types (*SI Appendix*, Fig. S7). One more layer was also added to this map to indicate the pathways in which the TFs are involved (*SI Appendix*, Table S6).

Discussion

Using the end-stage markers of lateral hypothalamic neurons, which are neuropeptides HCRT and MCH, we established their transcriptional machinery. To our knowledge this study is unique in purifying intact HCRT and MCH cells from late embryonic brains of mice. We identified molecules that might be the driving machinery of these neurons and used these markers as a guideline to develop protocols to establish these cells from mouse iPSCs.

Our aims were to establish a method to dissociate and culture live neurons and to have a specific marker to isolate specific cell types. With reporter proteins under specific promoters and quick aggregation method, it was possible to specifically purify them. Nevertheless, in the case of cell types with weak expression of

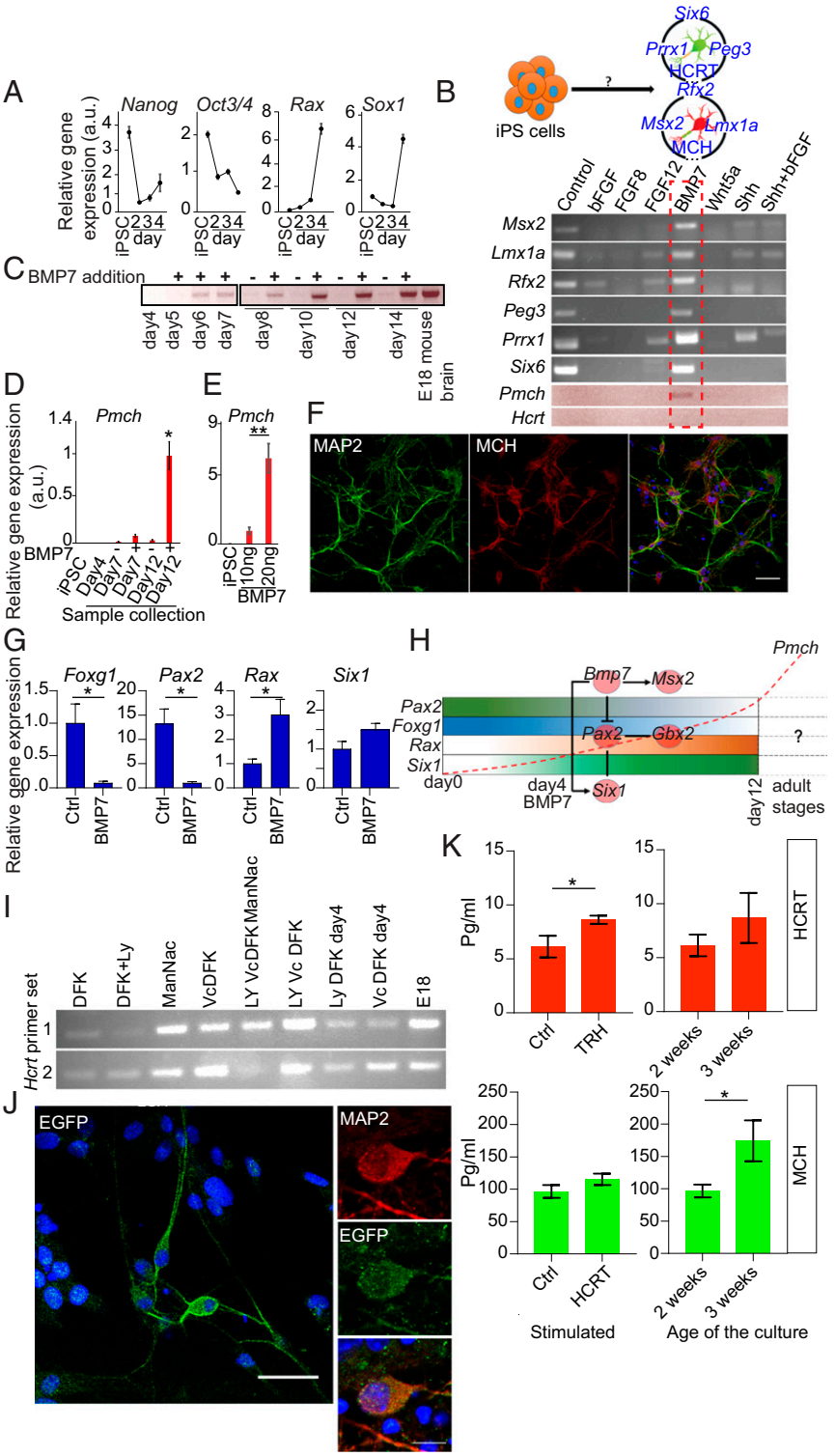

Fig. 6. Generation of HCRT and MCH neurons from iPSCs. (*A*) qRT-PCR for pluripotency (*Oct3/4*, *Nanog*), hypothalamic (*Rax*), and early neuroepithelial (*Sox1*) markers. A large decrease is observed in the expression level of pluripotent markers within 4 d while hypothalamic genes exhibit marked increase. (*B*, *Upper*) Schematic figure, which indicates that induction of candidate genes enriched in HCRT and MCH cells, with the help of a specific molecule or condition(?), might induce the expression of *Hcrt* and *Pmch* genes. (*Lower*) RT-PCR for TFs enriched in HCRT and MCH cells in cultures exposed to different signaling molecules and growth factors. iPSCs using protocol in *SI Appendix*, Fig. S5*F* were exposed to different molecules with potential role in the hypothalamus development. BMP7 showed strong potential to induce all indicated TFs and also *Pmch*. (*C*) The expression pattern of *Pmch* in the samples with and without BMP7 after different days in culture. Differentiating neurospheres were treated with and without 10 ng/mL BMP7 from day 4. Only in BMP7-treated samples a large expression of *Pmch* was observed and not in controls. (*D*) qRT-PCR for *Pmch* expression. Samples were treated as in *C*. (*E*) The effect of different concentrations of BMP7 on expression pattern of *Pmch*. Results show that the effect of BMP7 on the expression of *Pmch* is dose-dependent. (*F*) Neurospheres were kept in differentiation medium for 12 to 14 d before being dissociated and plated on PDL-coated dishes to produce mature neurons. Two weeks after plating the cells were stained for MCH and MAP2 expression. (*G*) qRT-PCR for representative genes among 30 tested genes downstream of *Bmp7*. (*H*) Schematic model of how TFs interact with each other to induce *Pmch* expression. For details see *Discussion*. (*I*) qRT-PCR for *Hcrt* expression under different differentiation conditions. The same method as for MCH differentiation was used to drive *Hcrt* expression except that ascorbic acid was used instead of BMP7 from day 3. Ascorbic acid induced *Hcrt* expression alone and in combination with other tested molecules (*SI Appendix*, Table S5). Due to short RNA sequence of the *Hcrt* gene, 2 different primer sets were used. (*J*) Hcrt-eGFP iPSC-derived, ascorbic acid-treated hypothalamic cells were stained for EGFP and MAP2 expression. (*K*) Two weeks after plating the neurospheres, differentiated HCRT and MCH cells were stimulated with TRH for HCRT and HCRT-1 for MCH cells for 3 h and the medium were collected to measure secreted molecules in the medium. Bar graphs show ELISA results for secretion analysis of HCRT and MCH neuropeptides. $*P = 0.04$ for HCRT and $P = 0.039$ for MCH; $**P < 0.01$; $n = 3$, mean ± SEM, *t* test. For *D*, *E*, *G*, and *K*: $*P < 0.05$; $**P < 0.01$. Scale bars: *F* and *J*, *Left*, 50 μm; *J*, *Right*, 10 μm.)

their specific markers the amplification of the reporter gene is required for which our developed method is of high efficiency.

We showed that the development of an intact hypocretin system requires PEG3, AHR, NR2F2, SIX6, PRRX1, and NKX6-2 as TFs, and that of the MCH system requires MSX2, GBX2, LMX1A, RFX2, SIX1, RAX, as well as PEG3. The respective role of these transcriptional factors in the development of HCRT and MCH needs further investigations by loss-of-function experiments in mice. Recently, in a comprehensive study by using single-cell sequencing (23), the molecular signatures of HCRT and MCH neurons in the adult mouse brain were identified, which can be complementary to our embryonic findings in constructing an overall transcriptional blueprint for these cell types. Although due to the developmental age differences we do not expect identical findings between these 2 studies, we did find important genes and TFs shared between the 2 for HCRT cells (*Slc17a6*, *Pdyn*, *Scg2*, *Rasgrp1*, and *Plagl1*). Interestingly, PLAGL1, which was recently reported to have a role in *Hcrt* transcription (51), is enriched in

both datasets, suggesting that this TF is substantially expressed from embryonic stage until adulthood and might be involved in controlling the *Hcrt* expression. We established the transcriptional machinery for these 2 cell types and illustrated the interaction of TFs with each other. The identified networks shed light on how these cell types might use their machinery during normal development and adult functioning. These networks might also explain how these cells integrate diverse inputs and function properly on demand. We subgrouped TFs for development, sleep, and feeding behavior and showed how they might interact with each other. The important role of LHX9 and EBF2 both in development and sleep are documented (24, 50), and we add here PEG3, which displayed a critical role in development and sleep. The precise fine-tuning of these networks during day and night guaranties the proper functioning of these cells that otherwise may lead to sleep disruption, obesity, and metabolic disorders.

Loss-of-function studies confirm the importance of our findings at the developmental level, indicating that the TFs found here are required for proper development of these cell types. Removal of the *Peg3* ortholog (*Zfp271*) totally abolished HCRT and MCH expression in zebrafish and deletion of the paternal allele of *Peg3* significantly decreased the number of HCRT and MCH neurons in mice. Note that *Zfp271* is an ortholog of *Peg3* and shares similarities to several other zinc finger proteins. Therefore, *Zfp271* in zebrafish may not be functionally identical to *Peg3* in mice. Additionally, the *Zfp271*-related sleep phenotype seen in zebrafish might be different in mice. We showed that knockdown of *Zfp271* affects locomotor activity in zebrafish; however, in mice it might affect other aspects of sleep, such as sleep fragmentation and the sleep EEG and not its total amount, as shown in $Hcrt^{KO/KO}$ mice. Such species differences need further investigation. *Peg3* is an imprinted gene with close connectivity to *Zim1* (52). It was established that the *Magel2* imprinted gene, which is similar to *Peg3*, a paternally expressed gene, also regulates *Hcrt* expression (53). *Peg3* has sex- and tissue-specific promoters (54) and is believed, like many other imprinted genes, to have a monoallelic pattern of expression, although it was shown recently that in some regions of the brain, specifically in the hypothalamus, there is a biallelic pattern of expression (55). Our finding that the deletion of the paternal allele significantly decreases but does not abolish the expression of HCRT and MCH suggests that some compensation mechanisms, including a role for the maternal allele, are at play. Furthermore, *Peg3* might play a role in the early development of HCRT and MCH neurons and not at the adult stage. How HCRT and MCH systems depend on imprinted genes and whether *Peg3* also depends on the core clock machinery remain to be discovered. The involvement of *Peg3* in the modulation of sleep in zebrafish seems dependent on its effect on *Hcrt* and *Mch* expression, but whether HCRT and MCH are the only affected cell types and whether both sexes are affected at the same level remains to be investigated, as it was shown that hypothalamic oxytocin neurons and maternal behavior are affected in *Peg3* female KO mice (43). *Peg3* in association with *Traf2* is involved in the TNF–NF-κB signal transduction pathway, which leads to cell survival or death (56). Therefore, it can be speculated that in some pathological conditions, such as in narcolepsy where HCRT neurons seem to be selectively destroyed, *Peg3* can participate in HCRT cell death.

The difficulties in accessing intact neurons from the human brain prompted us to establish protocols to produce these cells from iPSCs. We established iPSCs from mouse fibroblasts and differentiated them toward lateral hypothalamic cell types. We identified BMP7 as the master signaling molecule that regulates the main TFs of both cell types and the expression of *Pmch*. RNA-seq of MCH cells indicated that GBX2 is a TF up-regulated in these cells. *Gbx2* expression highly influences the expression of *Pax2* (57, 58), which itself is suppressed by BMP7 (Fig. 6*G*). *Six1*, which is also up-regulated by BMP7 treatment (Fig. 6*G*), has strong genetic interaction with *Pax2* (59). On the other hand, MSX2, which is the TF with the highest (5.5-fold change) overexpression in MCH cells, is highly expressed under BMP7 exposure (Fig. 6*B*). Based on these findings we propose a model for the generation of MCH cells from stem cells (Fig. 6*H*). This model suggests BMP7 as the major player in fate determination of MCH cells.

To induce the expression of the HCRT gene we applied vitamin C, of which its role in CNS development is well-documented. It was shown in the fetal rat brain that vitamin C increases from 374 μg/g on the 15th day of gestation to 710 μg/g by the 20th day and remains at this level until birth (60). Our findings are complementary and add induction markers to the other studies that successfully generated hypothalamic cells from human and mouse stem and iPSCs (48, 61–63). Since we derived HCRT neurons from *Hcrt-EGFP* mice expressing eGFP under the control of a 3.4-kb human Hcrt promoter (64), the generated cells may not be identical to the authentic mouse HCRT neurons. However, we believe that the authentic promoter is also activated as we reported the expression of *Hcrt* at mRNA and protein levels.

We identified genes and molecules which might have a role in the pathophysiology of narcolepsy with cataplexy. QRFP is the latest hypothalamic neuropeptide identified and implicated in feeding, locomotor activity, arousal, and metabolism (65–67). More recently QRFP and its receptor GPR103 were found to regulate sleep in zebrafish (42). Additionally, the QRFP receptor GPR103 heterodimerizes with HCRT receptors and is involved in protection against Alzheimer's disease (68). QRFP seems not to be colocalized with HCRT, suggesting that its reduced expression in *Hcrt-Ataxin-3* mice is secondary to the lack of HCRT cells. Since the expression of *Qrfp* is normal in $Hcrt^{KO/KO}$ mice, we speculate that its expression is under the control of other factors produced by HCRT neurons. A secondary reduction of QRFP in narcolepsy, if confirmed, may explain auxiliary symptoms, such as food intake behavior and obesity (30, 69). The fact that the identified TFs here are also highly enriched in the immune system suggests that more investigation on their role in the pathophysiology of narcolepsy with cataplexy is warranted.

Methods

Animals. Two mouse models of narcolepsy [$Hcrt^{ko/ko}$: B6.129S6-$Hcrt^{tm1Ywa}$/J and *Hcrt-ataxin-3*: B6;D2-Tg(HCRT-Ataxin-3)] were used to perform RNA sequencing of the different brain regions. *Hcrt-Cre* [B6;D2-Tg(HCRT-Cre-IRES-eGFP)] mice were used to purify HCRT cells and WT C57BL/6J mice were used for purification of MCH cells. *Hcrt-EGFP* (B6;D2-Tg(HCRT-eGFP)) mice were used to establish iPSCs. *Peg3* KO (129Sv.MF1-$Peg3^{Tm1}$) mice were used for HCRT and MCH staining and counting. All animals were back-crossed to C57BL/6J for at least 10 generations and provided by international collaborators, except for C57BL/6J mice, which were purchased from Charles Rivers Laboratory. Animals were maintained under standard animal housing conditions with free access to food and water. All experimental protocols were approved by the Veterinary Ethical commission of the state of Vaud, Switzerland.

RNA Sequencing. Transcriptome analysis from mouse models of narcolepsy were performed as described in Nikolaeva et al. (70) and aligned against *Mus musculus* GRCm38.75. The R package DESEQ2 was used for statistical tests. For sorted hypothalamic cells, double-stranded cDNA for RNA-seq library preparation was generated using SMART-Seq v4 Ultra Low Input RNA reagents (Catalog no. 634888, Clontech) according to the protocol provided with the reagents beginning with 2 ng (MCH cells) or 0.8 ng (for HCRT cells) of total RNA and using 11 cycles of PCR amplification. Next, 150 pg of the resulting cDNA were used for library preparation with the Illumina Nextera XT DNA Library reagents (Catalog no. 15032354, Illumina) using the single-cell RNA-seq library preparation protocol developed for the Fluidigm C1 (Fluidigm). Data analysis is summarized in *SI Appendix, Supplementary Information Text*.

Behavioral Assays. Sleep and activity of zebrafish were assessed based on refs. 41 and 42. Briefly, the behavioral tests were performed on zebrafish injected with 2.5 ng of *Zfp271*-Mo, or with H_2O as control. From 110 to 158 h post-fertilization, larval zebrafish were placed into a 96-well plate, 1 per well, in 300 μL of E3 embryo medium. Locomotor activity was analyzed by the video tracking module of the classic version of Zebrabox (Viewpoint Lifescience). The system applied a continuous infrared detection under a 14/10-h cycle of

light/dark. The quantification mode of Zebrabox was set up following the parameters described in Chen et al. (42): integration time bins, 1 min; detection threshold, 15; burst, 29; freeze, 3. Any 1-min epoch with less than 0.1 s of movement was considered as 1 min of sleep (42). Finally, a sleep bout was defined as a continuous string of sleep minutes. Data were processed using MATLAB.

ACKNOWLEDGMENTS. We thank the Genomic Technologies Facility of the University of Lausanne (Switzerland) for performing our RNA sequencing; and Dr. T. Sakurai for providing *Hcrt*$^{ko/ko}$, orexin-EGFP, orexin-Cre, and Hcrt-ataxin-3 mice. This work was supported by the Swiss National Science Foundation Grants 31003A_146615 and 31003A_173126 (to M.T.), and partially by grants from the NRJ Foundation and Blackswan Foundation (to M.T.).

1. M. W. Schwartz, S. C. Woods, D. Porte, Jr, R. J. Seeley, D. G. Baskin, Central nervous system control of food intake. *Nature* **404**, 661–671 (2000).
2. O. K. Hassani, P. Henny, M. G. Lee, B. E. Jones, GABAergic neurons intermingled with orexin and MCH neurons in the lateral hypothalamus discharge maximally during sleep. *Eur. J. Neurosci.* **32**, 448–457 (2010).
3. R. R. Konadhode *et al*., Optogenetic stimulation of MCH neurons increases sleep. *J. Neurosci.* **33**, 10257–10263 (2013).
4. G. C. Harris, M. Wimmer, G. Aston-Jones, A role for lateral hypothalamic orexin neurons in reward seeking. *Nature* **437**, 556–559 (2005).
5. C. Broberger, L. De Lecea, J. G. Sutcliffe, T. Hökfelt, Hypocretin/orexin- and melanin-concentrating hormone-expressing cells form distinct populations in the rodent lateral hypothalamus: Relationship to the neuropeptide Y and agouti gene-related protein systems. *J. Comp. Neurol.* **402**, 460–474 (1998).
6. C. F. Elias *et al*., Chemically defined projections linking the mediobasal hypothalamus and the lateral hypothalamic area. *J. Comp. Neurol.* **402**, 442–459 (1998).
7. C. Peyron *et al*., Neurons containing hypocretin (orexin) project to multiple neuronal systems. *J. Neurosci.* **18**, 9996–10015 (1998).
8. T. Sakurai *et al*., Orexins and orexin receptors: A family of hypothalamic neuropeptides and G protein-coupled receptors that regulate feeding behavior. *Cell* **92**, 573–585 (1998).
9. Y. Chen *et al*., Targeted disruption of the melanin-concentrating hormone receptor-1 results in hyperphagia and resistance to diet-induced obesity. *Endocrinology* **143**, 2469–2477 (2002).
10. J. Li, Z. Hu, L. de Lecea, The hypocretins/orexins: Integrators of multiple physiological functions. *Br. J. Pharmacol.* **171**, 332–350 (2014).
11. W. J. Giardino, L. de Lecea, Hypocretin (orexin) neuromodulation of stress and reward pathways. *Curr. Opin. Neurobiol.* **29**, 103–108 (2014).
12. S. Jego *et al*., Optogenetic identification of a rapid eye movement sleep modulatory circuit in the hypothalamus. *Nat. Neurosci.* **16**, 1637–1643 (2013).
13. M. Shimada, N. A. Tritos, B. B. Lowell, J. S. Flier, E. Maratos-Flier, Mice lacking melanin-concentrating hormone are hypophagic and lean. *Nature* **396**, 670–674 (1998).
14. G. Conductier *et al*., Melanin-concentrating hormone regulates beat frequency of ependymal cilia and ventricular volume. *Nat. Neurosci.* **16**, 845–847 (2013).
15. B. I. Baker, D. J. Bird, J. C. Buckingham, Salmonid melanin-concentrating hormone inhibits corticotrophin release. *J. Endocrinol.* **106**, R5–R8 (1985).
16. A. Adamantidis, L. de Lecea, A role for Melanin-Concentrating Hormone in learning and memory. *Peptides* **30**, 2066–2070 (2009).
17. L. Lin *et al*., The sleep disorder canine narcolepsy is caused by a mutation in the hypocretin (orexin) receptor 2 gene. *Cell* **98**, 365–376 (1999).
18. C. Peyron *et al*., A mutation in a case of early onset narcolepsy and a generalized absence of hypocretin peptides in human narcoleptic brains. *Nat. Med.* **6**, 991–997 (2000).
19. R. M. Chemelli *et al*., Narcolepsy in orexin knockout mice: Molecular genetics of sleep regulation. *Cell* **98**, 437–451 (1999).
20. R. S. Liblau, A. Vassalli, A. Seifinejad, M. Tafti, Hypocretin (orexin) biology and the pathophysiology of narcolepsy with cataplexy. *Lancet Neurol.* **14**, 318–328 (2015).
21. D. Latorre *et al*., T cells in patients with narcolepsy target self-antigens of hypocretin neurons. *Nature* **562**, 63–68 (2018).
22. D. Qu *et al*., A role for melanin-concentrating hormone in the central regulation of feeding behaviour. *Nature* **380**, 243–247 (1996).
23. L. E. Mickelsen *et al*., Single-cell transcriptomic analysis of the lateral hypothalamic area reveals molecularly distinct populations of inhibitory and excitatory neurons. *Nat. Neurosci.* **22**, 642–656 (2019).
24. J. Dalal *et al*., Translational profiling of hypocretin neurons identifies candidate molecules for sleep regulation. *Genes Dev.* **27**, 565–578 (2013).
25. J. Liu *et al*., Evolutionarily conserved regulation of hypocretin neuron specification by Lhx9. *Development* **142**, 1113–1124 (2015).
26. M. Honda *et al*., IGFBP3 colocalizes with and regulates hypocretin (orexin). *PLoS One* **4**, e4254 (2009).
27. V. Cvetkovic-Lopes *et al*., Elevated Tribbles homolog 2-specific antibody levels in narcolepsy patients. *J. Clin. Invest.* **120**, 713–719 (2010).
28. L. Yelin-Bekerman *et al*., Hypocretin neuron-specific transcriptome profiling identifies the sleep modulator Kcnh4a. *eLife* **4**, e08638 (2015).
29. L. E. Mickelsen *et al*., Neurochemical heterogeneity among lateral hypothalamic hypocretin/orexin and melanin-concentrating hormone neurons identified through single-cell gene expression analysis. *eNeuro* **4**, ENEURO.0013-17.2017 (2017).
30. J. Hara *et al*., Genetic ablation of orexin neurons in mice results in narcolepsy, hypophagia, and obesity. *Neuron* **30**, 345–354 (2001).
31. S. Gopalakrishnan, B. A. Sullivan, S. Trazzi, G. Della Valle, K. D. Robertson, DNMT3B interacts with constitutive centromere protein CENP-C to modulate DNA methylation and the histone code at centromeric regions. *Hum. Mol. Genet.* **18**, 3178–3193 (2009).
32. K. Okamoto *et al*., QRFP-deficient mice are hypophagic, lean, hypoactive and exhibit increased anxiety-like behavior. *PLoS One* **11**, e0164716 (2016).
33. R. A. Romanov *et al*., Molecular interrogation of hypothalamic organization reveals distinct dopamine neuronal subtypes. *Nat. Neurosci.* **20**, 176–188 (2017).
34. T. Matsuki *et al*., Selective loss of GABA(B) receptors in orexin-producing neurons results in disrupted sleep/wakefulness architecture. *Proc. Natl. Acad. Sci. U.S.A.* **106**, 4459–4464 (2009).
35. Y. Li, X. B. Gao, T. Sakurai, A. N. van den Pol, Hypocretin/Orexin excites hypocretin neurons via a local glutamate neuron-A potential mechanism for orchestrating the hypothalamic arousal system. *Neuron* **36**, 1169–1181 (2002).
36. T. Shimogori *et al*., A genomic atlas of mouse hypothalamic development. *Nat. Neurosci.* **13**, 767–775 (2010).
37. A. Weyer, K. Schilling, Developmental and cell type-specific expression of the neuronal marker NeuN in the murine cerebellum. *J. Neurosci. Res.* **73**, 400–409 (2003).
38. K. K. Kim, R. S. Adelstein, S. Kawamoto, Identification of neuronal nuclei (NeuN) as Fox-3, a new member of the Fox-1 gene family of splicing factors. *J. Biol. Chem.* **284**, 31052–31061 (2009).
39. J. A. González, E. Horjales-Araujo, L. Fugger, C. Broberger, D. Burdakov, Stimulation of orexin/hypocretin neurones by thyrotropin-releasing hormone. *J. Physiol.* **587**, 1179–1186 (2009).
40. F. Lu *et al*., Rax is a selector gene for mediobasal hypothalamic cell types. *J. Neurosci.* **33**, 259–272 (2013).
41. D. A. Prober, J. Rihel, A. A. Onah, R. J. Sung, A. F. Schier, Hypocretin/orexin overexpression induces an insomnia-like phenotype in zebrafish. *J. Neurosci.* **26**, 13400–13410 (2006).
42. A. Chen *et al*., QRFP and its receptors regulate locomotor activity and sleep in zebrafish. *J. Neurosci.* **36**, 1823–1840 (2016).
43. L. Li *et al*., Regulation of maternal behavior and offspring growth by paternally expressed Peg3. *Science* **284**, 330–333 (1999).
44. T. Wataya *et al*., Minimization of exogenous signals in ES cell culture induces rostral hypothalamic differentiation. *Proc. Natl. Acad. Sci. U.S.A.* **105**, 11796–11801 (2008).
45. G. Alvarez-Bolado, F. A. Paul, S. Blaess, Sonic hedgehog lineage in the mouse hypothalamus: From progenitor domains to hypothalamic regions. *Neural Dev.* **7**, 4 (2012).
46. H. Wichterle, I. Lieberam, J. A. Porter, T. M. Jessell, Directed differentiation of embryonic stem cells into motor neurons. *Cell* **110**, 385–397 (2002).
47. N. Maeda *et al*., Aortic wall damage in mice unable to synthesize ascorbic acid. *Proc. Natl. Acad. Sci. U.S.A.* **97**, 841–846 (2000).
48. K. Hayakawa *et al*., Epigenetic switching by the metabolism-sensing factors in the generation of orexin neurons from mouse embryonic stem cells. *J. Biol. Chem.* **288**, 17099–17110 (2013).
49. J. P. Silva *et al*., Regulation of adaptive behaviour during fasting by hypothalamic Foxa2. *Nature* **462**, 646–650 (2009).
50. A. K. De La Herrán-Arita *et al*., Aspects of the narcolepsy-cataplexy syndrome in O/E3-null mutant mice. *Neuroscience* **183**, 134–143 (2011).
51. S. Tanaka *et al*., Involvement of PLAGL1/ZAC1 in hypocretin/orexin transcription. *Int. J. Mol. Med.* **43**, 2164–2176 (2019).
52. A. Ye, H. He, J. Kim, Paternally expressed Peg3 controls maternally expressed Zim1 as a trans factor. *PLoS One* **9**, e108596 (2014).
53. S. V. Kozlov *et al*., The imprinted gene Magel2 regulates normal circadian output. *Nat. Genet.* **39**, 1266–1272 (2007).
54. B. P. Perera, J. Kim, Sex and tissue specificity of Peg3 promoters. *PLoS One* **11**, e0164158 (2016).
55. B. P. Perera, R. Teruyama, J. Kim, Yy1 gene dosage effect and bi-allelic expression of Peg3. *PLoS One* **10**, e0119493 (2015).
56. F. Relaix, X. J. Wei, X. Wu, D. A. Sassoon, Peg3/Pw1 is an imprinted gene involved in the TNF-NFkappaB signal transduction pathway. *Nat. Genet.* **18**, 287–291 (1998).
57. M. Hidalgo-Sánchez, R. Alvarado-Mallart, I. S. Alvarez, Pax2, Otx2, Gbx2 and Fgf8 expression in early otic vesicle development. *Mech. Dev.* **95**, 225–229 (2000).
58. T. Katahira *et al*., Interaction between Otx2 and Gbx2 defines the organizing center for the optic tectum. *Mech. Dev.* **91**, 43–52 (2000).
59. P. X. Xu *et al*., Six1 is required for the early organogenesis of mammalian kidney. *Development* **130**, 3085–3094 (2003).
60. C. C. Kratzing, J. D. Kelly, J. E. Kratzing, Ascorbic acid in fetal rat brain. *J. Neurochem.* **44**, 1623–1624 (1985).
61. K. Ogawa *et al*., Vasopressin-secreting neurons derived from human embryonic stem cells through specific induction of dorsal hypothalamic progenitors. *Sci. Rep.* **8**, 3615 (2018).
62. F. T. Merkle *et al*., Generation of neuropeptidergic hypothalamic neurons from human pluripotent stem cells. *Development* **142**, 633–643 (2015).
63. L. Wang *et al*., Differentiation of hypothalamic-like neurons from human pluripotent stem cells. *J. Clin. Invest.* **125**, 796–808 (2015).
64. A. Yamanaka *et al*., Hypothalamic orexin neurons regulate arousal according to energy balance in mice. *Neuron* **38**, 701–713 (2003).
65. N. Chartrel *et al*., The RFamide neuropeptide 26RFa and its role in the control of neuroendocrine functions. *Front. Neuroendocrinol.* **32**, 387–397 (2011).
66. S. Takayasu *et al*., A neuropeptide ligand of the G protein-coupled receptor GPR103 regulates feeding, behavioral arousal, and blood pressure in mice. *Proc. Natl. Acad. Sci. U.S.A.* **103**, 7438–7443 (2006).
67. K. Ukena, T. Osugi, J. Leprince, H. Vaudry, K. Tsutsui, Molecular evolution of GPCRs: 26Rfa/GPR103. *J. Mol. Endocrinol.* **52**, T119–T131 (2014).
68. J. Davies *et al*., Orexin receptors exert a neuroprotective effect in Alzheimer's disease (AD) via heterodimerization with GPR103. *Sci. Rep.* **5**, 12584 (2015).
69. A. Schuld, J. Hebebrand, F. Geller, T. Pollmächer, Increased body-mass index in patients with narcolepsy. *Lancet* **355**, 1274–1275 (2000).
70. S. Nikolaeva *et al*., Nephron-specific deletion of circadian clock gene Bmal1 alters the plasma and renal metabolome and impairs drug disposition. *J. Am. Soc. Nephrol.* **27**, 2997–3004 (2016).